Active Chicken Meat Packaging Based on Polylactide Films and Bimetallic Ag–Cu Nanoparticles and Essential Oil

Jasim Ahmed, Yasir Ali Arfat, Anibal Bher, Mehrajfatema Mulla, Harsha Jacob, and Rafael Auras

Abstract: Plasticized polylactide (PLA) composite films with multifunctional properties were created by loading bimetallic silver–copper (Ag–Cu) nanoparticles (NPs) and cinnamon essential oil (CEO) into polymer matrix via compression molding technique. Rheological, structural, thermal, barrier, and antimicrobial properties of the produced films, and its utilization in the packaging of chicken meat were investigated. PLA/PEG/Ag–Cu/CEO composites showed a very complex rheological system where both plasticizing and antiplasticizing effects were evident. Thermal properties of plasticized PLA film with polyethylene glycol (PEG) enhanced considerably with the reinforcement of NPs whereas loading of CEO decreased glass transition, melting, and crystallization temperature. The barrier properties of the composite films were reduced with the increase of CEO loading ($P < 0.05$). Their optical properties were also modified by the addition of both CEO and Ag–Cu NPs. The changes in the molecular organization of PLA composite films were visualized by FTIR spectra. Rough and porous surfaces of the films were evident by scanning electron microscopy. The effectiveness of composite films was tested against *Salmonella* Typhimurium, *Campylobacter jejuni* and *Listeria monocytogenes* inoculated in chicken samples, and it was found that the films loaded with Ag–Cu NPs and 50% CEO showed maximum antibacterial action during 21 days at the refrigerated condition. The produced PLA/Ag–Cu/CEO composite films can be applied to active food packaging.

Keywords: cinnamon essential oil, compression-molding, complex viscosity, nanocomposite, polylactide

Practical Application: The nanoparticles and essential oil loaded PLA composite films are capable of exhibiting antimicrobial effects against Gram (+) and (–) bacteria, and extend the shelf-life of chicken meat. The bionanocomposite films showed the potential to be manufactured commercially because of the thermal stability of the active components during the hot-press compression molding process. The developed bionanocomposites could have practical importance and open a new direction for the active food packaging to control the spoilage and the pathogenic bacteria associated with the fresh chicken meat.

Introduction

The responsible use of natural resources and the concerns about plastics' environmental pollution or safety of petrochemical-based packaging materials have galvanized researchers to develop biodegradable and environment-friendly polymers as an alternative to widely used plastics in the packaging industry. A trending approach to replace the fossil-derived materials is the use of eco-friendly materials. Biopolymers like polylactides (PLA) have been of increasing interest due to ease of production, the possibility of recycling and composting at the end of life, and commercial acceptance in various areas such as food packaging, biomedical applications, and automobile industry (Gao, Picot, Bilotti, & Peijs, 2017; Sung, Chang, & Han, 2017; Tawakkal, Cran, Miltz, & Bigger, 2014). However, PLA-based films are brittle/rigid, biologically inactive and possess poor barrier properties (Javidi, Hosseini, & Rezaei, 2016; Zhu, Tang, Yin, & Yang, 2018), which limit their applicability for food packaging films. In response to these drawbacks, development of nanocomposites has been investigated through some physical approaches such as the reinforcement of several kinds of nanofillers such as metallic nanoparticles and nanoclays into the biopolymer matrix to enhance physicomechanical, barrier and thermal properties of films (Jamshidian, Tehrany, Imran, Jacquot, & Desobry, 2010; Rhim, Park, & Ha, 2013). In a polymer blend, the compatibility among constituents with phase changes play an important role, which finally improved the thermomechanical and structural properties of the blend over the neat polymers. Several studies on polymer blends have indicated that their resulting properties were not only influenced by the distribution of monomers but also chemical constituents of the participating polymers (Rana, Mandal, & Bhattacharyya, 1993; Rana, Mandal, & Bhattacharyya, 1996). During thermal analysis, the presence of a single glass transition temperature is the key characteristics signifying the miscibility of polymer blends whereas a phase separation is obvious for immiscible polymers. Unlike to conventional polymeric blends, the miscibility of nanofillers into polymer matrices is studied differently. The T_g of nanocomposite films is mainly dependent on the type of interaction (attractive, repulsive, or neutral) between groups present between the nanofillers and the

JFDS-2017-1950 Submitted 11/29/2017, Accepted 2/16/2018. *Authors Ahmed, Arfat, Mulla, and Jacob are with Food and Nutrition Program, Environment & Life Sciences Research Center, Kuwait Inst. for Scientific Research, Safat, Kuwait. Authors Bher and Auras are with The School of Packaging, Michigan State Univ., East Lansing, Mich., U.S.A. Author Bher is also with Inst. Sabato, UNSAM-CNEA, San Martin, Buenos Aires, Argentina and with the Inst. de Materiales de Misiones (IMAM), CONICET-UNaM, Posadas, Misiones, Argentina. Direct inquiries to author Ahmed (E-mail: jaahmed@kisr.edu.kw).*

doi: 10.1111/1750-3841.14121

Journal of Food Science A Publication of the Institute of Food Technologists

polymer chains. The composite materials based on PLA and reinforced with single metal NPs like ZnO, TiO_2, and Ag have been characterized by numerous researchers (Murariu et al., 2011; Zhuang, Liu, Zhang, Hu, & Shen, 2009). Recently, monometallic NPs (for example, Ag, Cu) have been alloyed to produce bimetallic (Ag/Cu) NPs with improved thermal, optical, interfacial and antimicrobial properties (Perdikaki et al., 2016; Tan & Cheong, 2013. Among the metal NPs, silver–copper (Ag–Cu) nanoalloys showed strong antibacterial activity with low loading concentrations as compared to single metal NPs like Ag or Cu (Taner, Sayar, Yulug, & Suzer, 2011; Zain, Stapley, & Shama, 2014). It has been established that NPs exhibited a strong antimicrobial activity; however, few reports are available on the nanoparticle resistant microorganisms (Scandorieiro et al., 2016; Graves Jr et al., 2015). Therefore, studies are sought to overcome the on-going problems on NP resistant organisms by following a combination of selected antimicrobial agents (Scandorieiro et al., 2016). A loading of NPs and naturally derived essential oils (EOs) into the PLA matrix could be the best strategy for the inactivation of food-borne pathogens. Scandorieiro et al. (2016) further reported that a blend of Ag NP with oregano essential oil resulted from an additive and synergistic antimicrobial activities against the multidrug-resistant bacterial strains namely, *E. coli*, *A. baumannii*, and methicillin-resistant *Staphylococcus aureus* (MRSA) strains. Moreover, the incorporation of EOs with antioxidant and antimicrobial properties into the film matrix diminishes uncertainties regarding their toxicity and safe use in food products (Holley & Patel, 2005). Among various EOs, cinnamon essential oil (CEO)—a rich source of cinnamaldehyde and eugenol active compounds has remarkable antibacterial, antioxidant, and antifungal activities (Oussalah, Caillet, Saucier, & Lacroix, 2007). Additionally, active compounds like cinnamaldehyde and eugenol obtained from cinnamon are recognized as generally recognized as safe (GRAS) materials. A limited number of studies have been carried out on PLA-based packaging added with either nanoparticles or EOs; however, no report is available on the compression-molded PLA/NP/EO films and its characterization. Additionally, there is no consensus among researchers whether a synergism or antagonism effect occurs against pathogens when both nanoparticles and essential oils are incorporated into the packaging materials. This work has been carried out to address the issue.

In this study, plasticized PLA based films incorporated with bimetallic NPs and CEO were prepared using the compression-molding technique. The study aimed to prepare plasticized PLA/NPs/CEO composite films with antimicrobial properties, which were further evaluated for chicken meat packaging applications. The effect of Ag–Cu NPs and CEO on the rheological and thermal properties as well as color and transparency of plasticized PLA was also studied.

Materials and Methods

Materials

Polylactide (PLA) (Ingeo™ Biopolymer 4043D) was obtained from NatureWorks LLC, USA. Pellets were vacuum dried during 24 hr at 60 °C before used. Polyethylene glycol (PEG) - M_n = 1,500 Da, cinnamon oil (Ceylon type; Product Number: W229202; Appearance: yellow to dark brown; refractive index at 20 °C: 1.529 to 1.537 and specific gravity: 1.030 to 1.050) and Ag–Cu NPs (Product Number: 576824; Appearance: grey to brown to black, and particle size: <100 nm) were bought from Sigma-Aldrich, U.S.A.

Strains and media used for microbiological test

Microbial strains of Gram (-) *Campylobacter jejuni* (ATCC 33291) and *Salmonella enterica sv* Typhimurium (ATCC 14028) and Gram (+) *Listeria monocytogenes* (ATCC 19114) were purchased from Remel Europe Limited (Kent, U.K.) and MediMark Europe (Grenoble, France). Media, Muller hinton agar (MHA), brain heart infusion broth (BHIB), tryptic soy broth (TSB), PALCAM agar base or polymyxin-acriflavin-lithium chloride-ceftazidime-aesculin-mannitol, CampyGen™ gas generation sachet, laked horse blood, PALCAM selective supplements, campylobacter selective agar base, xylose lysine deoxycholate agar (XLD), preston campylobacter selective and growth supplements were all obtained and produced as previously described (Ahmed, Mulla, & Arfat, 2017).

Preparation of compression molded PLA and composite films

(i) PLA-PEG/Ag-Cu (98/2 and 96/4) were compounded using a batch mixer Brabender® ATR Plasticorder (Brabender Instruments, Inc., NJ, U.S.A.) outfitted with 50 cm^3 mixing cell and torque recorder, at 180 °C, 80 rpm, during 5 min followed by compression molding with a thicknesses of 1 mm on a hot press (PHI QL438-C, City of Industry, CA, U.S.A.) at 172 °C by operating with a force of 25 tons for 5 min, and finally cooled on a cold press to room temperature.

(ii) PLA-PEG and CEO blend at a ratio of 2:1 was compounded by a twin-screw extruder - screw L/D ratio: 42 and screw speed: 80 rpm (Century ZSK-30 (Century, Traverse City, MI, U.S.A.)). The temperature for the master-batch formulation ranged between 160 and 180 °C in the different zones. The extruded mass was pelletized in a BT 25 pelletizer (Bay City, MI, U.S.A.), oven dried at 50 °C and 3 hr in, then stored at −15 °C until use. Ag-Cu and PLA/CEO master batch were also mixed and compression molded in composite films (PLA/CEO/Ag-Cu 64/32/4) as described in step (i).

(iii) Neat plasticized PLA films were prepared by the method described in step (i & ii) with slight temperature modifications and used as a control.

The prepared films were stored at cold room (4 ± 0.5°C) for 150 days for microbial validation (*in vitro*).

Characterization of the films' properties

Rheological measurements and thickness. A micrometer from Mituyoto Corp., Japan was used to determine the films' thickness at different positions (n = 10) with a sensitivity of 0.001 mm. Three films were used for the measurement.

Rheological measurements of the plasticized PLA and the composites films were studied with an advanced rheometer (Discovery HR-3, from TA Instruments, U.S.A.) operating an electrically heated plate (EHP) with a diameter of 25 mm. The temperatures selected for the experiments were 160, 170, 180, and 190 °C, and the gap between the two plates was maintained at 500-mm. The samples were positioned between two plates and allowed to reach the set temperature for approximately 5 min before testing. Dynamic frequency-sweep (0.1 to 10 Hz) and time sweep (0 to 1800 s; frequency of 1 Hz) experiments were done in the LVR region (that is, linear viscoelastic response), with a constant strain of 0.05%. All rheological data were acquired for duplicate samples from the software attached to the instrument.

Barrier properties. Water vapor permeability (WVP) was acquired with a Permatran W3/31 (Mocon Inc., MN, U.S.A.) at

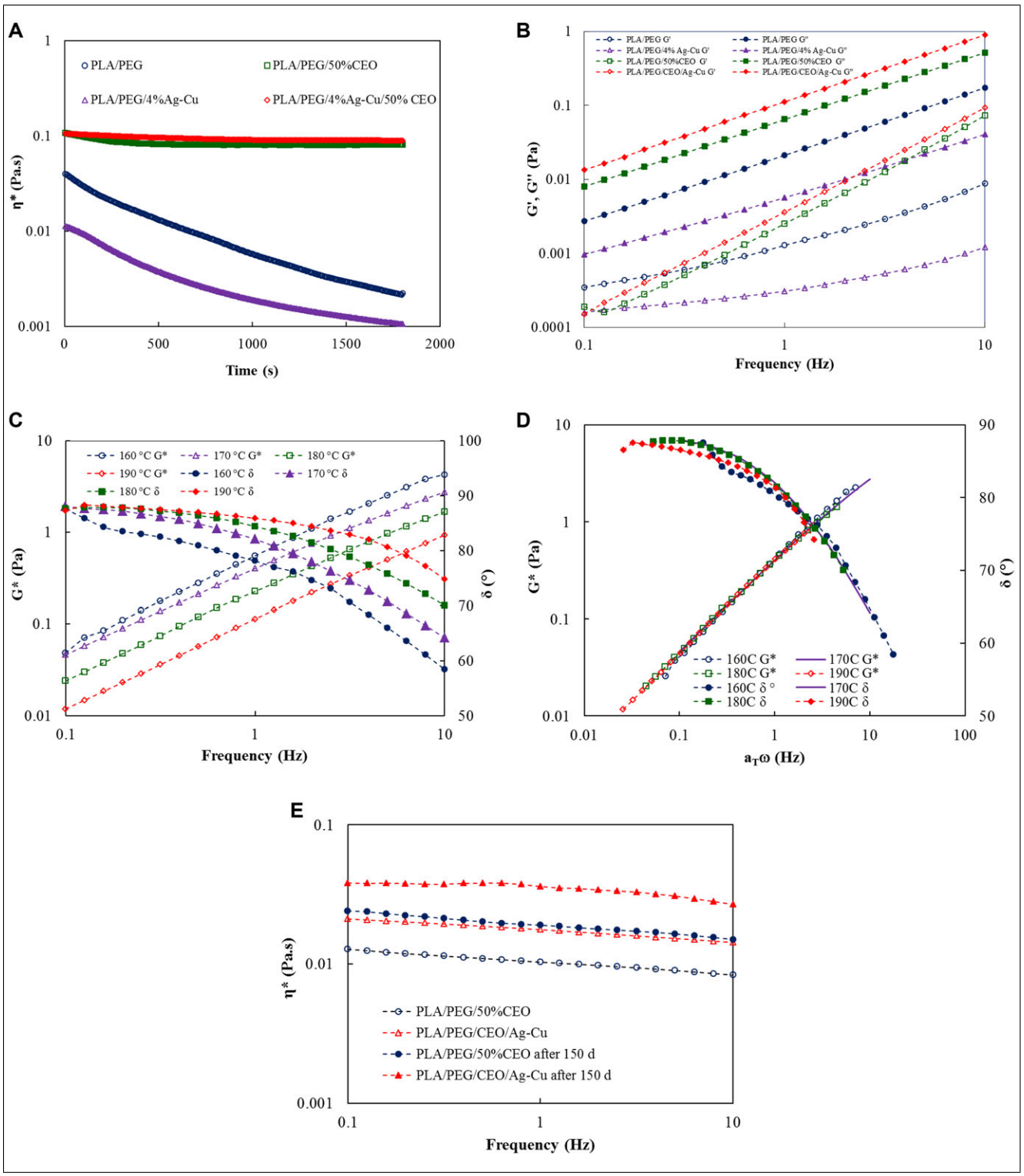

Figure 1–Time dependency of PLA composite films as influenced by nanoparticles and essential oil (A). Effect of nanoparticles and essential oil on the mechanical spectra of plasticized PLA at 180 °C as a function of frequency (B). Effect of temperature on complex modulus and phase angle values of PLA/PEG/4% Ag-Cu/50% CEO composites with frequency (C). Generation of master curve for the composites at a reference temperature of 170 °C (D). Effect of storage period on mechanical rigidity of antimicrobial films (E).

23 °C with 50 ± 1% RH following the ASTM standard F1249 (ASTM, 1995a). The O_2 permeability (OP) of the films was obtained using an Extra-Solution Permeo$_2$ instrument from Capannori (LU, Italy) at 23 °C and 50 ± 1% RH following the ASTM D3985-05 procedure (ASTM, 1995b). Measurements of WVP and OP were conducted in triplicate using three different set of films.

Optical properties. A Hunter tristimulus colorimeter from Hunter laboratory, VA, U.S.A. was selected to measure the color of the films (i.e., L^* indicating lightness, a^* indicating the degree

of redness to greenness, and b^* indicating the degree of yellowness to blueness values). The total color difference (ΔE^*) was estimated following the method described elsewhere (Ahmed et al., 2017). The light transmittance in the UV (200, 280, and 350 nm) and visible (400, 500, 600, 700, and 800 nm) wavelength regions was obtained using a spectrophotometer (Thermo Scientific, U.S.A.). The transparency value (TV) of the film was based on our earlier work (Ahmed et al., 2017). The color and optical properties were measured in triplicate using three different set of films.

Fourier transform infrared (FTIR) spectroscopy. The FTIR measurements of three different set of films were obtained in an attenuated total reflectance using a Nicolet FTIR Spectrometer (iS5, Thermo Scientific). Each spectrum was gathered between 550 and 4000 cm^{-1} with a resolution of 4 cm^{-1}. Reported spectra contain mean values over three replicated.

X-ray diffraction (XRD). XRD was conducted on an Advance diffractometer from Bruker D8, Germany with a Cu-Kα source (wavelength: 0.154 nm) at 40 kV and 250 mA. The 2θ values ranged between 5° and 80°. Measurements were conducted in two samples.

Thermal properties. The melting temperature, T_m (from the first heating cycle), and crystallization (T_c) and glass transition temperatures (T_g) – (from the second cycle) were obtained as previously described (Ahmed, Mulla, & Arfat, 2016). The enthalpy and the crystallinity (% X_c) were calculated using the instrumental software (Universal Analysis). Triplicate measurements were conducted from three set of films.

Morphology. A scanning electron microscope (SEM) model JCM-6000 Plus from JEOL, Japan was used for assessment of surface morphology of film samples. The films were coated with a thin conductive layer of the brass stub and sputtered with gold using a current of 10 kV, and photographs at 300× magnification were obtained. Three different films were used for the measurement.

***In vitro* antibacterial effectiveness of PLA composite films.** *S.* Typhimurium (Gram (–)), *C. jejuni* (Gram (–)), and *L. monocytogenes* (Gram - (+)) were employed to assess the antimicrobial activity of the films (after day 1 and 150 days of storage) using the liquid culture test (Ahmed, Hiremath, & Jacob, 2016b; Ahmed, Mulla, & Arfat, 2016). Briefly, methods are described here. For *Salmonella* and *Listeria*, a disc of a film (0.4 g) was sterilized using UV light and immersed in a test tube containing 10 mL TSB. The TSB was inoculated with 0.1 mL (1×10^8 CFU/mL) inoculum and incubated at 25 °C with shaking at 200 rpm. One milliter of the inoculated medium was sampled after 24 hr, and a serial dilution method was employed for spreading onto BHIA plates. The inoculated plates were incubated @ 37 °C for 24 hr, and the cell concentrations were counted as colony-forming units (CFU). The PLA/PEG film was kept as a control. For *C. jejuni,* a film disc was placed in a test tube containing 10 mL BHIB and 0.1 mL of *C. jejuni* inoculum were added (1×10^8 CFU/mL). The test tubes were incubated at 42 °C for 48 hr. Then, 1 mL aliquots were serially diluted with BHIB and 0.1 mL spread plated onto Campylobacter agar plates. The organisms were grown at 42 °C for 48 hr under microaerophilic conditions and the cell concentrations were counted as CFU. For assessment of the microbial inactivation efficiency of the film, three samples were chosen for each treatment and three measurements were carried out for each sample.

Confirmation test with chicken. The antimicrobial effectiveness of PLA and PLA/Ag-Cu/CEO films was tested in chicken as a model food system against *S.* Typhimurium, *C. jejuni*, and *L. monocytogenes* following the method described by Ahmed et al. (2016). Briefly, 3 sets of sterilized minced chicken samples (≈10 g) were put in different petri dishes. An aliquot of a 1×10^8 CFU/mL inoculum of S. Typhimurium, *C. jejuni* and *L. monocytogenes* were added into each petri dish, spread over the minced chicken, and hold for 30 min. Afterwards, minced chicken inoculated with test organisms were wrapped individually with the selected films (8 × 8 cm), and stored at 4 °C. All samples were tested for the presence of *S.* Typhimurium, *L. monocytogenes* or *C. jejuni* at different time intervals (0, 7, 14, and 21 days). Chicken samples wrapped in neat PLA/PEG films served as a control sample.

For counting, the films were removed from the chicken sample, homogenized for 2 min in 10 mL of sterile peptone water (0.1 % w/v) for *S.* Typhimurium or *L. monocytogenes* and 10 mL of sterile BHIB (0.1 % w/v) for *C. jejuni*. Homogenates (0.1 mL) were spread-plated on PALCAM agar for *L. monocytogenes*, XLD agar for S. Typhimurium and on Campylobacter agar plates for *C. jejuni*, respectively. Plates were incubated at 37 °C for 48 hr *(L. monocytogenes*), 24 hr (*S.* Typhimurium) and at 42 °C for 48 hr under microaerophilic conditions (*C. jejuni*) before strain counting and reported as log CFU/g of chicken. All tests were evaluated in duplicate and repeated twice ($n = 4$).

Statistical analysis

The data were analyzed with the SPSS software (SPSS 17.0, SPSS Inc., Ill., U.S.A.) through the analysis of variance (ANOVA).

Results and Discussion

Rheological measurements and thickness

The thickness of compression-molded PLA films incorporated with Ag–Cu NPs and CEO is shown in Table 1 The composite films had the same thickness than the neat plasticized PLA film ($P > 0.05$).

Time sweep tests were first used to examine the thermal stability of neat plasticized and composite PLA films due to PLA's sensitivity to thermal degradation. The compression molded (CM) PLA composites thermal stability was measured by employing dynamic frequency time sweep tests, so that we could observe any changes with time in their complex viscosity at a constant 170 °C and 1 Hz. Figure 1A shows that the melt composites films behave differently with time. The η^* of PLA/PEG degraded dramatically between 0.04 and 0.002 Pa.s (≈95%) during a holding period of 30 min, and the degradation was somewhat restricted (≈91%) by a loading of Ag-Cu in the PLA/PEG blend indicating that the PLA composites exhibited time dependency with a substantial reduction in the mechanical property. A significant drop in PLA's viscosity after 30 to 40 min holding period was reported (Murariu, Murariu, Raquez, Bonnaud, & Dubois, 2015; Ahmed et al., 2016; Nofar, Heuzey, Carreau, & Kamal, 2016). The thermal degradation mostly happens at temperatures that are very close to and above the melting temperature one (Gerard & Budtova, 2012). Those authors opined that metal oxide incorporation into the PLA matrix at temperatures closed to melt processing is conduced to the "unzipping" depolymerization leading to considerable degradation of the molecular weight of the PLA. Incorporation of CEO into the PLA/PEG matrix produced a composite almost time-independent, and the time independency was more obvious for CM PLA/PEG/Ag-Cu/CEO melt.

Frequency sweeps of plasticized PLA composites are shown in Figure 1B. All studied composites show predominantly liquid-like

Table 1–Thickness, water vapor, and oxygen permeabilities of compression-molded plasticized PLA films incorporated with Ag–Cu NPs and CEO.

Film sample	Thickness (mm)	Water vapor permeability (g mm/m^2 day atm)	Oxygen permeability (cc mm/m^2 day atm)
Control PLA/PEG (90/10)	0.182 ± 0.005^a	26.9 ± 2.1^c	22.8 ± 1.6^b
PLA/PEG/2% Ag-Cu NPs	0.183 ± 0.004^a	20.6 ± 1.4^d	17.9 ± 1.2^c
PLA/PEG/4% Ag-Cu NPs	0.184 ± 0.005^a	16.0 ± 1.2^e	14.0 ± 0.7^d
PLA/PEG/25% CEO	0.183 ± 0.004^a	32.6 ± 2.8^b	24.9 ± 2.1^b
PLA/PEG/50% CEO	0.185 ± 0.003^a	40.1 ± 2.2^a	32.1 ± 3.6^a
PLA/PEG/4% Ag-Cu NPs/50% CEO	0.186 ± 0.005^a	30.7 ± 3.0^{bc}	23.6 ± 1.8^b

Values are given as mean ± SD ($n = 3$).
Different superscript letters in the same column indicates significant differences ($P < 0.05$).

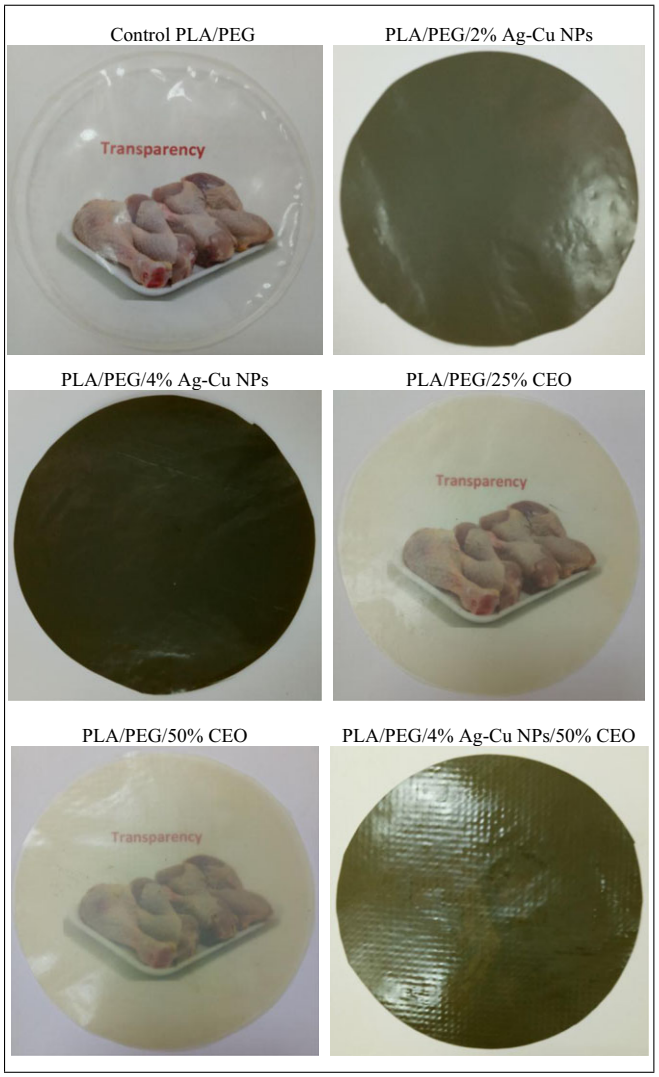

Figure 2–Appearance/transparency of compression-molded plasticized PLA films incorporated with Ag–Cu NPs and cinnamon essential oil.

behavior ($G'' > G'$) throughout the frequency range. While Ag–Cu nanoparticles (NP) were added to the PLA/PEG blend, the elastic modulus, G' and the viscous modulus, G'' dropped significantly, and it indicates that the metallic NPs acted as a catalyst for the degradation of the blend above the melting temperature. Degradation of PLA in the presence of nanoparticles has been evident in the literature, and even it is recommended the use of silane-treated metallic oxide surface to prevent the degradation (Arfat, Ahmed, Al Hazza, Jacob, & Joseph, 2017). Mostly, it has found that at a higher filler concentration, G' does not depend on the frequency at low frequencies, which could indicate a solid-like behavior (Bhatia, Gupta, Bhattacharya, & Choi, 2009). However, when we added 4% Ag–Cu, the G' of the PLA nanocomposites do not considerably illustrate this effect.

CEO incorporation into PLA/PEG, however, improved both the moduli significantly, and the increasing trend continued for the composites loaded with NPs and CEO. PLA/PEG/Ag–Cu and PLA/PEG/CEO composites showed the typical terminal behavior with the scaling law (that is, $G' \propto \omega^2$ and $G'' \propto \omega$). It suggests better affinity of CEO for PLA/PEG blend compared to Ag–Cu NPs. Indeed, the PLA/PEG/Ag–Cu/CEO composites represented a very complex rheological system where both plasticizing and antiplasticizing effects were evident, and it is attributed by the presence of PEG, CEO, and NPs, respectively. Furthermore, it can be argued that the essential oil could make a thick layer on the film surface (although volatiles evaporated) that restricted the melting of the PLA/PEG blend, and improved the mechanical properties. However, this observation is in contrast to our earlier observations on solvent cast PLA/PEG/CEO composites where addition of CEO into the PLA/PEG matrix acted as an extra plasticizer and reduced both dynamic moduli abruptly (Ahmed et al., 2016). Similar CEO induced plasticization effect has been reported in the literature (Lee, Lee, & Song, 2015).

PLA/PEG/Ag–Cu/CEO composites' complex shear modulus (G^*) and phase angle (δ) were plotted against frequency at selected temperatures (Figure 1C). It shows that the G^* decreased and the δ augmented as the process temperature increased between 160 and 190 °C due to shear-thinning of the NC. The G^*-ω rheograms showed a similar pattern with increasing temperature, and the slopes were varied between 0.90 and 0.97. All rheograms were shifted into G^* and δ master curves by employing time-temperature-superposition principle at 170 °C—use as reference temperature (Figure 1C) following the method described by Ahmed (2017). As it can be seen that the reduced frequency, $a_T\omega$ extended to a lower range, and G^*-ω rheograms were superimposed adequately with longer relaxation time. However, it can be seen that the rheograms for δ–-ω in the lower frequency range were not superimposed adequately especially at the lowest and the highest temperatures employed for the experiments since at low-frequencies or high temperatures an additional relaxation mechanism involving morphological changes could occur. The failure of superposition suggests an incompatibility of CEO and Ag–Cu NPs with the plasticized PLA/PEG blend in the melt. While we produced a master curve for PLA/PEG/Ag–Cu and PLA/PEG/CEO

Table 2–Color, light transmittance and transparency values of compression-molded plasticized PLA films incorporated with Ag-Cu NPs and CEO.

Film sample	Color parameters											
	L^*			a^*			b^*			ΔE^*		
Control PLA/PEG (90/10)	91.20 ± 0.06^{a}			−1.49 ± 0.04^{c}			0.04 ± 0.01^{f}			2.14 ± 0.18^{f}		
PLA/PEG/2% Ag–Cu NPs	43.15 ± 0.29^{b}			−0.31 ± 0.07^{a}			10.19 ± 0.23^{c}			51.60 ± 0.44^{c}		
PLA/PEG/4% Ag–Cu NPs	40.11 ± 0.12^{c}			−0.20 ± 0.06^{a}			13.27 ± 0.15^{b}			55.25 ± 0.27^{b}		
PLA/PEG/25% CEO	91.32 ± 0.14^{a}			−1.8 ± 0.13^{d}			3.6 ± 0.12^{e}			4.61 ± 0.13^{e}		
PLA/PEG/50% CEO	91.41 ± 0.25^{a}			−2.19 ± 0.19^{e}			4.08 ± 0.09^{d}			5.60 ± 0.21^{d}		
PLA/PEG/4% Ag–Cu NPs/50% CEO	40.35 ± 0.26^{c}			−1.27 ± 0.10^{b}			14.83 ± 0.11^{a}			57.33 ± 0.24^{a}		
	Light transmittance (%)											Transparency value
	200	280	350	400	500	600	700	800				
Control PLA/PEG (90/10)	0.12 ± 0.02^{a}	48.63 ± 0.53^{a}	70.14 ± 0.32^{a}	81.18 ± 0.44^{a}	84.87 ± 0.67^{a}	85.38 ± 0.25^{a}	86.46 ± 0.27^{a}	86.91 ± 0.39^{a}				0.38 ± 0.03^{f}
PLA/PEG/2% Ag–Cu NPs	0.04 ± 0.01^{b}	7.31 ± 0.26^{b}	8.64 ± 0.28^{c}	11.45 ± 0.21^{d}	12.37 ± 0.29^{d}	14.79 ± 0.17^{d}	15.87 ± 0.13^{d}	16.63 ± 0.18^{d}				4.54 ± 0.09^{c}
PLA/PEG/4% Ag–Cu NPs	0.02 ± 0.01^{b}	6.37 ± 0.18^{c}	7.45 ± 0.09^{d}	10.84 ± 0.16^{e}	11.53 ± 0.14^{e}	12.69 ± 0.11^{e}	14.70 ± 0.25^{e}	15.46 ± 0.27^{e}				4.87 ± 0.07^{b}
PLA/PEG/25% CEO	0.03 ± 0.01^{b}	0.14 ± 0.02^{d}	13.80 ± 0.13^{b}	59.64 ± 0.37^{b}	68.33 ± 0.48^{b}	71.72 ± 0.52^{b}	73.67 ± 0.98^{b}	74.96 ± 0.61^{b}				0.79 ± 0.02^{e}
PLA/PEG/50% CEO	0.00 ± 0.00^{c}	0.08 ± 0.01^{d}	6.29 ± 0.06^{e}	47.53 ± 0.35^{c}	60.85 ± 0.31^{c}	64.44 ± 0.43^{c}	66.86 ± 0.51^{c}	68.91 ± 0.30^{c}				1.03 ± 0.09^{d}
PLA/PEG/4% Ag–Cu NPs/50% CEO	0.00 ± 0.00^{c}	0.0 ± 0.00^{d}	0.00 ± 0.00^{f}	3.12 ± 0.16^{f}	4.25 ± 0.08^{f}	5.68 ± 0.16^{f}	6.21 ± 0.17^{f}	6.66 ± 0.12^{f}				6.62 ± 0.26^{a}

Values are given as mean ± SD ($n = 3$).
Different superscript letters in the same column indicate significant differences ($P < 0.05$).

separately at a reference temperature of 170 °C (not shown), and a similar failure of the TSS with more scattered data, in particular, Ag–Cu loaded composite, was observed. We could attribute this finding to the limited flow of the polymer chains in the molten state produced by the addition of nanoparticles to the PLA matrix. The NC sample showed shear-thinning behavior, at high-frequency regions ($a_T\omega > 1$ Hz). At high frequency, alignment of the NPs can happen, and the presence of NPs has just almost no effect on the dynamic moduli of the PLA nanocomposite and relaxation mechanism. At this stage, the polymer matrix mostly controls the deformation. According to Haley and Lodge (2004), small intramolecular contributions to local composition are enough to produce time-temperature superposition failure. The applicability of the TTS principle for PLA/PEG/Ag–Cu/CEO samples is an indication of thermorheological simplicity of the composites upon which it exhibits the predictability of these materials' rheological characteristics when subjected to a wide range of temperatures (Dealy & Plazek 2009; Distefano & Pister, 1972).

The mechanical strength of the PLA/PEG/Ag–Cu/CEO composite films was monitored up to 150 days as shown in Fig. 1E. As expected, the η^* of both CEO containing films were increased twofold, which is believed to be associated with the evaporation of CEO on the course of the storage period, and the film became more rigid. It suggests that the antimicrobial films could not be used for food packaging after a longer period of manufacturing.

Barrier properties

WVP and OP values of compression-molded PLA based films loaded with Ag–Cu NPs and CEO are presented in Table 1. The WVP and OP values obtained for the control plasticized PLA are comparable to previous reports (Martino, Jimenez, & Ruseckaite, 2009; Rhim et al., 2013) whereas the values for Ag–Cu reinforced films were reduced significantly. This trend was ascribed to the increase in a tortuous path, which causes disruptions in the diffusion of O_2 and H_2O across the PLA composite film. However, both WVP and OP of composite films loaded with CEO were higher than that of control film ($P < 0.05$). Barrier properties could be influenced by several factors like water or oxygen sensitivity and crystallinity. The reduced crystallinity of CEO loaded composite films (discussed later) might have a role in increasing permeability values. Loading of hydrophobic CEO could affect the cohesion forces of PLA network, and thus it could enhance water vapor or oxygen transport through the film matrix. These results matched the findings of Rojas-Graü et al. (2006) who described that EOs loaded into biopolymer films increase the permeability of the produced films as non-polar ingredients such as EOs and lipids can act as poor gas barriers.

Optical properties of films

The appearance of compression-molded plasticized PLA films incorporated with Ag–Cu NPs and CEO are illustrated in Fig. 2. The change in color values was pronounced when NPs were reinforced into the PLA matrix as shown by the ΔE^* values (Table 2). The L^* considerably dropped to less than half of the L^* measured for the plasticized PLA film, and a^* and b^* values augmented ($P < 0.05$). These changes in the color parameters could be accredited by the characteristic surface plasmon resonance of the Ag-Cu NPs (Varshney, Bhadauria, & Gaur, 2010). These results were also found by Rhim et al. (2013) who reported that Ag nanoparticles markedly increased a^*, b^*, and ΔE^*-values and decreased L^*- values of agar-silver nanocomposites. With the

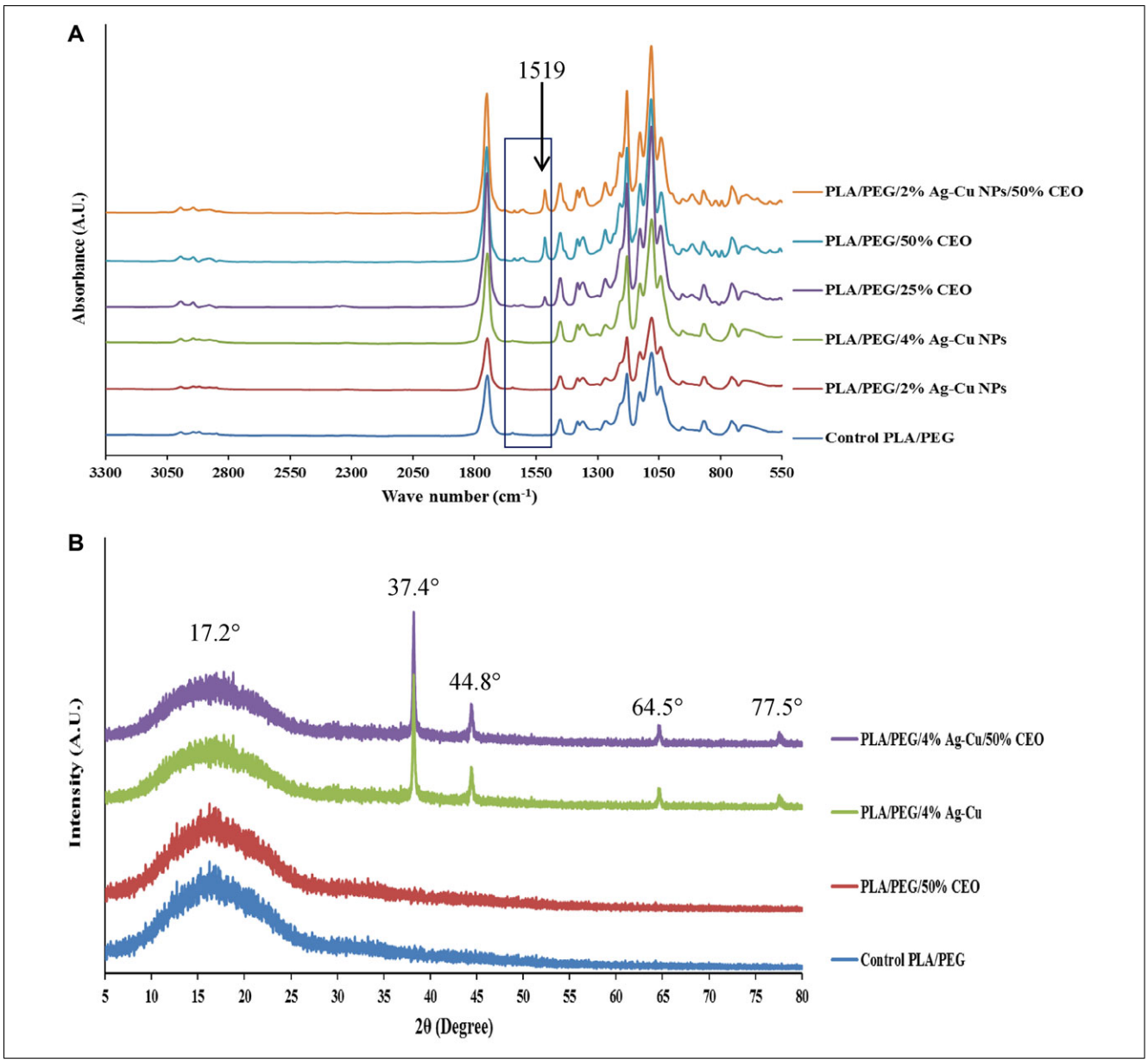

Figure 3–FTIR spectra (A) and X-ray diffraction patterns (B) of compression-molded plasticized PLA films incorporated with Ag–Cu NPs and cinnamon essential oil.

incorporation of CEO in the PLA films, L^* values do not change whereas the color a^* and b^* values changes considerably suggesting an increase in greenness and yellowness. These changes in color values have been accredited to coloring ingredients of CEO ($a^* = -0.18$ and $b^* = 1.75$). Similar effects on color due to the addition of essential oils into PLA have been reported by Qin, Li, Liu, Yuan, and Li (2017).

Table 2 shows the light transmission (at UV and visible wavelengths) and transparency values of compression-molded PLA based composite films. The control plasticized PLA film exhibited the highest %T at 600 nm (85.38%) with a poor anti-UV property (280 nm: 48.63%; 350 nm: 70.14%). After incorporation of Ag-Cu NPs or CEO into the plasticized PLA matrix, the light transmittance of the films decreased at all wavelengths in a dose-dependent manner. However, the films incorporated with both Ag–Cu NPs and CEO showed lowest %T. This drop in %T is attributed to the light scattering due to the presence of the Ag–Cu NPs and coloring components in CEO droplets dispersed in the polymer matrix (Arfat, Benjakul, Prodpran, Sumpavapol, Songtipya, 2016). Therefore, this is an edge contributed to Ag–Cu NPs and CEO, making the composite films viable as packaging films for UV and light sensitive food products. A similar trend in %T of whey protein nanocomposite films was reported by Sothornvit, Hong, An, and Rhim (2010). The TV of the compression-molded plasticized PLA film increased after incorporation of Ag-Cu NPs and CEO ($P < 0.05$), indicating a lower transparency of the produced films.

FTIR spectroscopy

Figure 3A shows the FTIR spectra of PLA films added with NPs and CEO. The FTIR spectra of neat plasticized PLA film exhibited characteristic peaks at 3000-2887 and 1757 cm^{-1}, representing the C-H stretching vibrations of the $-CH_3$ group and $-C=O$ of the ester group of PLA, respectively (Gong et al., 2014; Haafiz et al., 2013). The asymmetric (1453 cm^{-1}) and symmetric (1359 cm^{-1})

Table 3–Thermal properties of compression-molded plasticized PLA films incorporated with Ag–Cu NPs and CEO.

Film sample	T_g (°C)	T_m (°C)	ΔH_m (J/g)	T_c (°C)	ΔH_c (J/g)	X_c (%)
Control PLA/PEG (90/10)	34.1 ± 0.6^b	150.0 ± 0.3^a	14.2 ± 0.2^c	90.2 ± 0.9^a	19.2 ± 0.7^c	20.6 ± 0.9^c
PLA/PEG/2% Ag–Cu NPs	40.1 ± 0.6^a	151.0 ± 0.4^a	19.9 ± 0.3^a	87.6 ± 0.6^b	22.5 ± 0.3^b	24.2 ± 0.6^b
PLA/PEG/4% Ag–Cu NPs	39.9 ± 0.5^a	150.9 ± 0.4^a	20.1 ± 0.2^a	88.1 ± 0.4^b	23.8 ± 0.2^a	26.5 ± 0.3^a
PLA/PEG/25% CEO	27.6 ± 0.9^c	140.8 ± 0.7^b	14.8 ± 0.4^c	75.0 ± 0.7^c	14.4 ± 0.1^e	18.0 ± 0.9^d
PLA/PEG/50% CEO	10.5 ± 0.5^e	131.2 ± 0.8^d	12.9 ± 0.3^d	69.0 ± 0.4^e	11.8 ± 0.3^f	13.7 ± 0.5^f
PLA/PEG/4% Ag–Cu NPs/50% CEO	14.9 ± 0.6^d	134.3 ± 0.7^c	18.2 ± 0.6^b	73.6 ± 0.5^d	15.3 ± 0.1^d	14.9 ± 0.2^e

Values are given as mean ± SD ($n = 3$).
Different superscript letters in the same column indicate significant differences ($P < 0.05$).

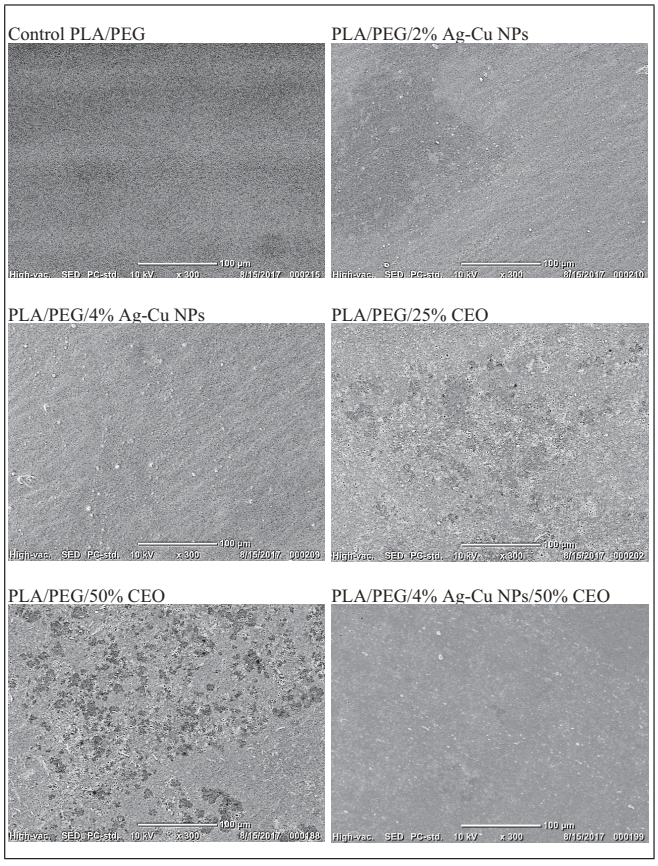

Figure 4–Scanning electron micrographs of compression-molded plasticized PLA films incorporated with Ag–Cu NPs and cinnamon essential oil. Magnification: ×300.

absorption peaks are attributed to the CH_3 deformation vibrational peaks of PLA (Chieng, Ibrahim, Yunus, & Hussein, 2013). Also, the peaks detected at the wavenumbers of 1181 and 1130 cm^{-1} were attributed to the symmetric C–O–C stretching of PLA ester group and -CH3 rocking mode, respectively (Kister, Cassanas, & Vert, 1998). The absorption band for asymmetric C-O-C stretching vibration was observed at 1091 cm^{-1}. The peaks ascribed to C-CH_3 and C-COO stretching vibrations were observed at 1047 and 870 cm^{-1}, respectively (Gong et al., 2014). No new peaks were evident due to the reinforcement of Ag–Cu NPs in the film matrix, which may indicate that there was only physical interaction between plasticized PLA and Ag–Cu NPs. Qu, Gao, Wu, and Zhang (2010) reported similar results for PLA based nanocomposite films. However, the FTIR spectra revealed a different peak at 1519 cm^{-1} when CEO was loaded into the PLA film matrix indicating a chemical interaction between plasticized PLA and CEO. The aromatic region with N–H bending vibration is evident by the band at 1519 cm^{-1} (Ahmed et al., 2016).

XRD analysis

Figure 3B shows the XRD patterns of compression-molded PLA composite films. The neat plasticized PLA films revealed a wide intensity with a maximum peak at $\sim 2\theta = 17°$, representing the semi-crystallinity structure of PLA (Pluta, 2004). Plasticized PLA film reinforced with Ag-Cu NPs exhibited four diffraction peaks corresponding to the (111), (200), (220), and (311) plane reflections of Ag-Cu NPs placed at $2\theta = 37.4°$, 44.8°, 64.8°, and 77.5° (Ahmed, Arfat, Castro-Aguirre, & Auras, 2016c). This spectrum indicated the presence of the Ag–CU NPs with a small variation of intensity of the $2\theta = 17°$ peak. Loading of CEO did not also affect the basic amorphous structure of PLA films after compression molding. Other authors also demonstrated that the biopolymer film structure was not affected by adding EO (Abdollahi, Rezaei, & Farzi, 2012; Atef, Rezaei, & Behrooz, 2015). Nevertheless, the PLA peak at $\sim 2\theta = 17°$ varied in strength with NP and CEO loading.

Thermal properties

The plasticized PLA film exhibited a T_g, T_m, and melt enthalpy around 34.1 °C, 150 °C, and 14.2 J/g, respectively (Table 3). Reinforcement of NPs increased the T_g of the resultant composite films by almost 6 °C and produces a significant change in the enthalpy. Such increase in T_g could be attributed to the restriction of polymeric chain mobility when bimetallic nanoparticles with the large specific surface area are reinforced into the matrix (Ahmed et al., 2016c). A significant increase in T_g of PLA based films reinforced with various nanoparticles has been reported (Cacciotti, Fortunati, Puglia, Kenny, & Nanni, 2014). The reinforcement of Ag–Cu NPs into plasticized PLA improved T_c and X_c; indicating decreased polymer chain movement and flexibility. A similar increase in T_c and X_c induced by reinforcement of nanoparticles has been reported (Fortunati et al., 2012).

Loading of CEO into the plasticized PLA films enhanced PLA chains molecular mobility and decreased the thermal properties in a dose-dependent manner. The T_g and T_m decreased significantly from 34.1 to 10.5 °C and 150.0 to 131 °C with 50% CEO in the composite films. Addition of CEO imparted a plasticization effect, which was in agreement with the rheological studies as discussed earlier. The T_c and $\%X_c$ followed a similar trend. These changes in thermal properties of CEO loaded PLA films are attributed to the ease in PLA crystallization at lower temperatures (Martin & Averous, 2001). A similar behavior in thermal properties of biopolymer/EO composite films has been reported (Javidi et al., 2016; Qin et al., 2017). However, Yahyaoui, Gordobil, Díaz, Abderrabba, and Labidi (2016) reported a small change

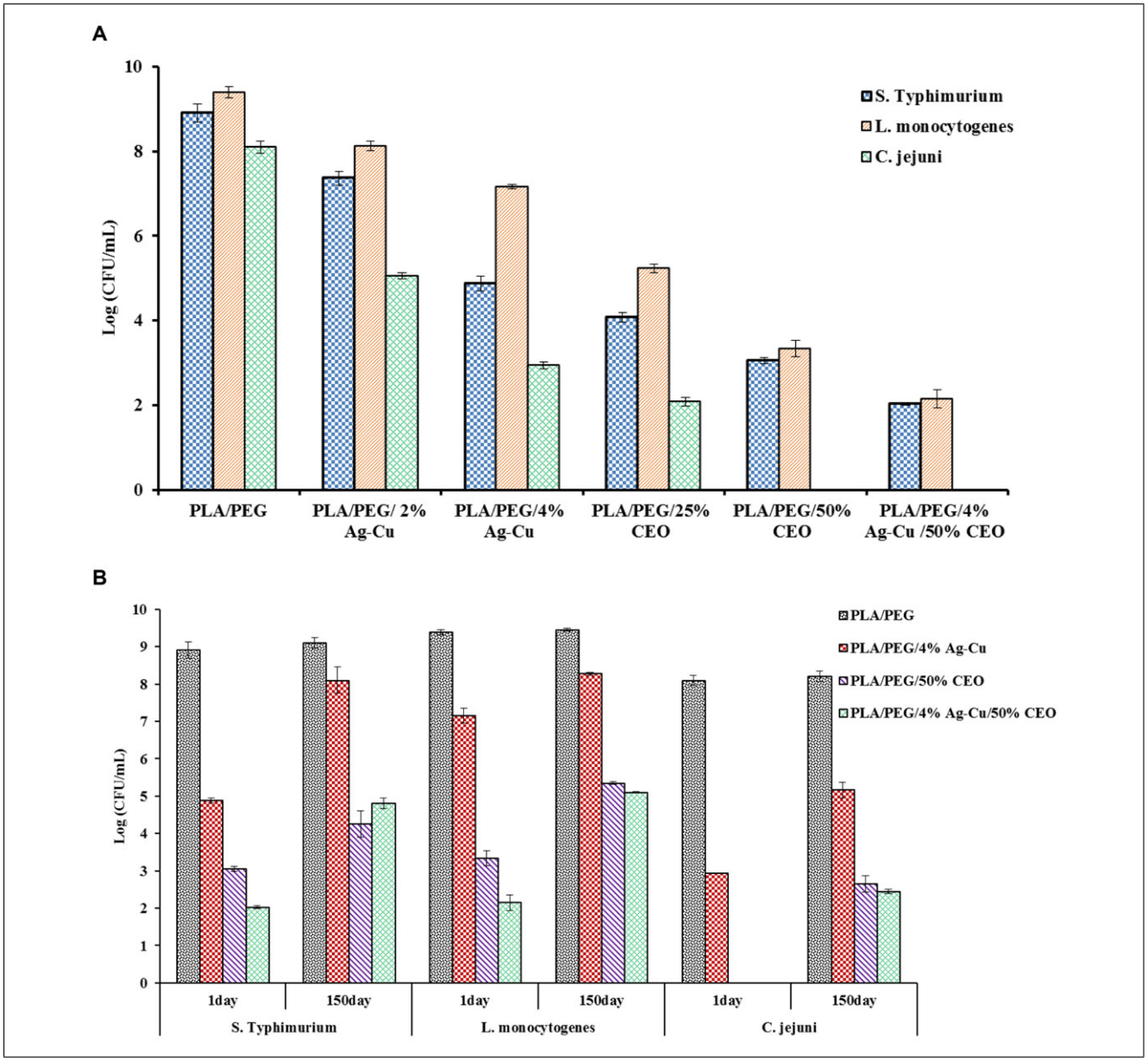

Figure 5–*In vitro* antibacterial activities of compression-molded PLA films incorporated with Ag–Cu NPs and CEO against *L. monocytogenes*, *S.* Typhimurium and *C. jejuni* after incubation for 1 (A) and 150 days (B).

in T_c with an increase of crystallinity for PLA/EO films produced with myrtle, thyme oils, and rosemary. They proposed the molecular structure and composition of the essential oils (Eucalyptol, Camphor, and α-pinene) play a vital role in the polymer chain mobility, and consequently, it behaved contrarily from other EO loaded polymer matrix.

Film morphology

Figure 4 illustrates the microstructure of compression-molded PLA composite films. The control plasticized PLA films had a non-porous surface structure confirming the good compatibility of PLA and PEG (Figure 4A). Loading of NPs into polymer matrix occasioned a coarse structure of the composite film and dispersed NPs (shown as white spots in the surface SEM image). With the loading of CEO, the film surface changed into a rough perforated structure with some distinct pores. The development of spongy structure was attributed to the CEO evaporation from PLA/CEO matrix during film development. Javidi et al. (2016) reported that EOs incorporated in the PLA polymer matrix caused a discontinuous film structure due to evaporation of volatile components happening during the drying of the films. The porosity of CEO loaded composite films decreased with 4% NPs reinforcement, signifying fine structural integrity.

Antimicrobial activities of compressed molded plasticized PLA composite films

The *in vitro* antimicrobial properties of plasticized PLA films and Ag–Cu NPs and CEO against *S.* Typhimurium, *L. monocytogenes,* and *C. jejuni* are shown in Figure 5. As expected, no antimicrobial activity was noticed for the control film after 24 hr of incubation whereas, the film loaded with NPs or CEO showed a significant reduction of all test microorganisms. However, the

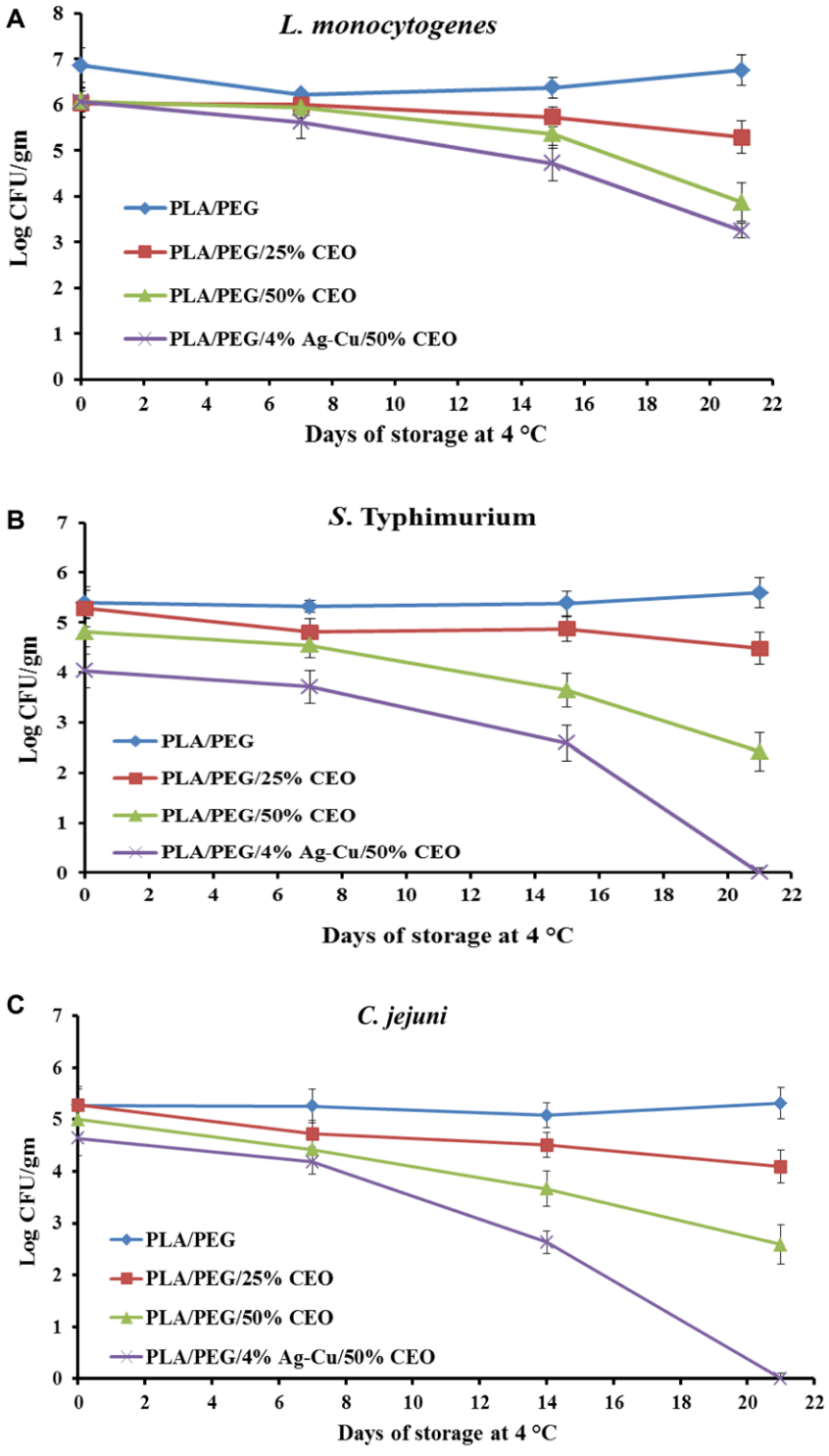

Figure 6–Growth of *L. monocytogenes*, *S.* Typhimurium and *C. jejuni* in chicken meat samples wrapped with compression-molded control PLA and PLA composite films and stored at 4 °C for 21 days.

films with 50% CEO showed strong inhibition against *C. jejuni* and the numbers were below the detection level (<10 CFU/mL). The higher antimicrobial effect of CEO loaded films can be attributed to the volatile nature of CEO making it release faster than NPs, and the high load of CEO used in this test. The quantity of antibacterial agent liberated from the film and the quantity of antibacterial agent on the surface of the film controls the inhibitory effect of the films against the test microorganism. Amongst all films, those incorporated with 50% CEO and 4% NPs exhibited the strongest antimicrobial activity and reduced the growth of *S.* Typhimurium, *L. monocytogenes* and *C. jejuni* by 6.89, 7.24, and 8.10 log10 CFU/mL, respectively. The excellent antimicrobial activity and mechanisms of action of Ag-Cu NPs and essential oils against various bacterial species have been demonstrated (Arfat, Benjakul, Prodpran, Sumpavapol, & Songtipya, 2014; Burt, 2004). The release of Ag^{+} or Cu^{2+} ions from the PLA films

could penetrate the cell wall and create a reaction with key cellular ingredients, which lastly lead to cell death. Furthermore, cinnamaldehyde, the main compound present in the CEO, can inhibit production of essential enzymes, stimulate protein denaturation and damage microbial cell wall permeability (Sanla-Ead, Jangchud, Chonhenchob, & Suppakul, 2012).

Antimicrobial activity of films PLA/PEG/4% Ag-Cu, PLA/PEG/50% CEO, and PLA/PEG/4% Ag-Cu/50% CEO was tested for their antimicrobial activity against selected pathogens after 150 days storage at 4 °C. The observed results are shown in Figure 5B. It can be seen that the antimicrobial activity of the films decreased after 150 days storage because of the high volatility and evaporation of CEO active components during storage of the films having less active compound (Hili, Evans, & Veness, 1997; Li, Kong, & Wu, 2013). The drop in the antimicrobial activity in the NP incorporated films could be influenced by the prolonged storage when the films become stiff that hindered the release of the NPs.

Microbial validity of the compressed molded PLA composite films with chicken sample

Figure 6 shows the degree of survival of *L. monocytogenes*, *S.* Typhimurium and *C. jejuni* in contaminated chicken in PLA composite packaging films during 21 days of refrigerated storage conditions. *L. monocytogenes*, *S.* Typhimurium and *C. jejuni*, average initial counts for the inoculated chicken samples were 6.65, 5.40, and 5.52 log CFU/g, respectively. The growth of all test microorganisms was controlled if cinnamon oil was incorporated in the PLA composite films. The counts of *L. monocytogenes*, *C. jejuni*, and *S.* Typhimurium decreased significantly to 3.87, 2.59, and 2.42 log CFU/g when packed in the film loaded with 50% CEO. Qin et al. (2015) also observed pronounced reduction in the microbial count of mushrooms when they were packed in PLA blend film incorporated with 9 wt% cinnamaldehyde.

The counts of *C. jejuni* and *S.* Typhimurium in chicken sample packed in PLA/Ag-Cu4%/CEO50% reached below the detection level on the 21st day. A considerably higher reduction of microorganisms was attributed to the synergistic effect triggered by the release of both cinnamaldehyde and silver/copper ions from the composite film which leads to disruption of metabolic processes or rupture of the bacterial cell wall, causing cell death (Li et al., 2010). Echegoyen and Nerín (2013) studied the migration of silver nanoparticles from nanocomposite films, and they described two mechanisms for the migration of silver nanoparticles, which were the detachment of the silver nanoparticles from the nanocomposites and dissolution of silver ions upon oxidation. These authors also concluded that the Ag migration was well below the maximum migration limits as stated by the European Union legislation. Cushen, Kerry, Morris, Cruz-Romero, and Cummins (2014) also studied the effect of time and temperature on the migration of silver and copper from polyethylene nanocomposite films to boneless chicken breasts, and they also showed that silver migration limits were below the values stated by the European Union legislation.

Conclusions

We produced active PLA composite films by incorporating Ag–Cu NPs and CEO via compression-molding method. Frequency sweep tests of plasticized PLA composites showed predominantly liquid-like behavior. Incorporation of NPs and CEO greatly influenced the barrier and structural properties of PLA nanocomposite films. Both Ag–Cu NPs and CLO influenced thermal properties of plasticized PLA films. The interaction between PLA matrix and Ag–Cu NPs was physical whereas chemical interactions were observed between PLA and CLO as revealed by FTIR spectroscopy. PLA composite films showed strong antimicrobial activity against all test microorganisms on contaminated chicken meat samples during 21 days at 4 °C. Overall, the PLA based composite films had the potential for development of UV protective and antimicrobial packaging material inhibiting the development of food borne pathogens.

Acknowledgments

The work was sponsored and supported by the KFAS and KISR (Grant #: FB087C).

References

Abdollahi, M., Rezaei, M., & Farzi, G. (2012). A novel active bionanocomposite film incorporating rosemary essential oil and nanoclay into chitosan. *Journal of Food Engineering*, *111*, 343–350.

Ahmed, J. (2017). Time-temperature-superposition principles: Application in biopolymer and food rheology. In J. Ahmed, P. Ptaszek, & S. Basu (Eds.), *Advances in food rheology and its applications* (pp. 209–241). UK: Woodhead Publishing.

Ahmed, J., Arfat, Y. A., Castro-Aguirre, E., & Auras, R. (2016c). Mechanical, structural and thermal properties of Ag–Cu and ZnO reinforced polylactide nanocomposite films. *International Journal of Biological Macromolecules*, *86*, 885–892.

Ahmed, J., Hiremath, N., & Jacob, H. (2016b). Antimicrobial, rheological, and thermal properties of plasticized polylactide films incorporated with essential oils to Inhibit *Staphylococcus aureus* and *Campylobacter jejuni*. *Journal of Food Science*, *81*, 419–429.

Ahmed, J., Mulla, M. Z., & Arfat, Y. A. (2016). Thermo-mechanical, structural characterization and antibacterial performance of solvent casted polylactide/cinnamon oil composite films. *Food Control*, *69*, 196–204.

Ahmed, J., Mulla, M., & Arfat, Y. A. (2017). Application of high-pressure processing and polylactide/cinnamon oil packaging on chicken sample for inactivation and inhibition of *Listeria monocytogenes* and *Salmonella* Typhimurium, and post-processing film properties. *Food Control*, *78*, 160–168.

Arfat, Y. A., Ahmed, J., Al Hazza, A., Jacob, H., & Joseph, A. (2017). Comparative effects of untreated and 3-methacryloxypropyltrimethoxysilane treated ZnO nanoparticle reinforcement on properties of polylactide-based nanocomposite films. *International Journal of Biological Macromolecules*, *101*, 1041–1050.

Arfat, Y. A., Benjakul, S., Prodpran, T., Sumpavapol, P., & Songtipya, P. (2014). Properties and antimicrobial activity of fish protein isolate/fish skin gelatin film containing basil leaf essential oil and zinc oxide nanoparticles. *Food Hydrocolloids*, *41*, 265–273.

Arfat, Y. A., Benjakul, S., Prodpran, T., Sumpavapol, P., Songtipya, P. (2016). Physico-mechanical characterization and antimicrobial properties of fish protein isolate/fish skin gelatin-zinc oxide (ZnO) nanocomposite films. *Food and Bioprocess Technology*, *9*(1), 101–112.

ASTM. (1995a). Standard test method for water vapor transmission rate through plastic film and sheeting using a modulated infrared sensor. In *Annual book of American standard testing methods*, F1249. Philadelphia, Pa.: ASTM.

ASTM. (1995b). Standard test method for oxygen gas transmission rate through plastic film and sheeting using a coulometric sensor. In *Annual book of American standard testing methods*, D3985. Philadelphia, Pa.: ASTM.

Atef, M., Rezaei, M., & Behrooz, R. (2015). Characterization of physical, mechanical, and antibacterial properties of agar-cellulose bionanocomposite films incorporated with savory essential oil. *Food Hydrocolloids*, *45*, 150–157.

Bhatia, A., Gupta, R. K., Bhattacharya, S. N., & Choi, H. J. (2009). An investigation of melt rheology and thermal stability of poly (lactic acid)/poly (butylene succinate) nanocomposites. *Journal of Applied Polymer Science*, *114*, 2837–2847.

Burt, S. (2004). Essential oils: Their antibacterial properties and potential applications in foods—A review. *International Journal of Food Microbiology*, *94*, 223–253.

Cacciotti, I., Fortunati, E., Puglia, D., Kenny, J. M., & Nanni, F. (2014). Effect of silver nanoparticles and cellulose nanocrystals on electro-spun poly(lactic) acid mats: Morphology, thermal properties and mechanical behavior. *Carbohydrate Polymers*, *2014*, 22–31.

Chieng, B. W., Ibrahim, N. A., Yunus, W. M. Z.W., & Hussein, M. Z. (2013). Plasticized poly (lactic acid) with low molecular weight poly (ethylene glycol): Mechanical, thermal, and morphology properties. *Journal of Applied Polymer Science*, *130*, 4576–4580.

Cushen, M., Kerry, J., Morris, M., Cruz-Romero, M., & Cummins, E. (2014). Evaluation and simulation of silver and copper nanoparticle migration from polyethylene nanocomposites to food and an associated exposure assessment. *Journal of Agricultural and Food Chemistry*, *62*(6)1403–1411.

Dealy, J. M., & Plazek, D. (2009). Time temperature superposition—A users guide. *Rheology Bulletin*, *78*(2), 16–31

Distefano, N. J., & Pister, K. S. (1972). On the identification problem for thermo-rheologically simple materials. *Acta Mechanica*, *13*, 179–190.

Echegoyen, Y., & Nerin, C. (2013). Nanoparticle release from nano-silver antimicrobial food containers. *Food and Chemical Toxicology*, *62*, 16–22.

Fortunati, E., Armentano, I., Zhou, Q., Puglia, D., Terenzi, A., Berglund, L. A., & Kenny, J. M. (2012). Microstructure and nonisothermal cold crystallization of PLA composites based on silver nanoparticles and nanocrystalline cellulose. *Polymer Degradation and Stability*, *97*, 2027–2036.

Gao, Y., Picot, O. T., Bilotti, E., & Peijs, T. (2017). Influence of filler size on the properties of poly (lactic acid)(PLA)/graphene nanoplatelet (GNP) nanocomposites. *European Polymer Journal*, *86*, 117–131.

Gerard, T., & Budtova, T. (2012). Morphology and molten-state rheology of polylactide and polyhydroxyalkanoate blends. *European Polymer Journal*, *48*, 1110–1117.

Gong, X., Pan, L., Tang, C. Y., Chen, L., Hao, Z., Law, W. C., . . . Wu, C. (2014). Preparation, optical and thermal properties of CdSe–ZnS/poly (lactic acid)(PLA) nanocomposites. *Composites Part B: Engineering*, *66*, 494–499.

Graves Jr, J. L., Tajkarimi, M., Cunningham, Q., Campbell, A., Nonga, H., Harrison, S. H., & Barrick, J. E. (2015). Rapid evolution of silver nanoparticle resistance in *Escherichia coli*. *Frontiers in Genetics*, *6*, 42

Haafiz, M. M., Hassan, A., Zakaria, Z., Inuwa, I. M., Islam, M. S., & Jawaid, M. (2013). Properties of polylactic acid composites reinforced with oil palm biomass microcrystalline cellulose. *Carbohydrate Polymers, 98*, 139–145.

Haley, J. C., & Lodge, T. P. (2004). Failure of time-temperature superposition in dilute miscible polymer blends. *Colloid and Polymer Science*, *282*, 793–801.

Hili, P., Evans, C. S., & Veness, R. G. (1997). Antimicrobial action of essential oils: The effect of dimethylsulphoxide on the activity of cinnamon oil. *Letters in Applied Microbiology*, *24*, 269–275.

Holley, R. A., & Patel, D. (2005). Improvement in shelf-life and safety of perishable foods by plant essential oils and smoke antimicrobials. *Food Microbiology*, *22*, 273–292.

Jamshidian, M., Tehrany, E. A., Imran, M., Jacquot, M., & Desobry, S. (2010). Poly-lactic acid: Production, applications, nanocomposites, and release studies. *Comprehensive Reviews in Food Science and Food Safety*, *9*, 552–571.

Javidi, Z., Hosseini, S. F., & Rezaei, M. (2016). Development of flexible bactericidal films based on poly (lactic acid) and essential oil and its effectiveness to reduce microbial growth of refrigerated rainbow trout. *LWT - Food Science and Technology*, *72*, 251–260.

Kister, G., Cassanas, G., & Vert, M. (1998). Effects of morphology, conformation and configuration on the IR and Raman spectra of various poly (lactic acid)s. *Polymer*, *39*, 267–273.

Lee, J.-H., Lee, J., Song, K. B. (2015). Development of a chicken feet protein film containing essential oils. *Food Hydrocolloids, 46*, 208–215.

Li, W. R., Xie, X. B., Shi, Q. S., Zeng, H. Y., You-Sheng, O. Y., & Chen, Y. B. (2010). Antibacterial activity and mechanism of silver nanoparticles on *Escherichia coli*. *Applied Microbiology and Biotechnology*, *85*, 1115–1122.

Li, Y. Q., Kong, D. X., & Wu, H. (2013). Analysis and evaluation of essential oil components of cinnamon barks using GC–MS and FTIR spectroscopy. *Industrial Crops and Products*, *41*, 269–278.

Martin, O., & Averous, L. (2001). Poly (lactic acid): Plasticization and properties of biodegradable multiphase systems. *Polymer*, *42*, 6209–6219.

Martino, V. P., Jimenez, A., & Ruseckaite, R. A. (2009). Processing and characterization of poly (lactic acid) films plasticized with commercial adipates. *Journal of Applied Polymer Science*, *112*, 2010–2018.

Murariu, M., Doumbia, A., Bonnaud, L., Dechief, A. L., Paint, Y., Ferreira, M., . . . Dubois, P. (2011). High-performance polylactide/ZnO nanocomposites designed for films and fibers with special end-use properties. *Biomacromolecules*, *12*, 1762–1771.

Murariu, M., Murariu, O., Raquez, J. M., Bonnaud, L., & Dubois, P. (2015). Current progress in the production of PLA–ZnO nanocomposites: Beneficial effects of chain extender addition on key properties. *Journal of Applied Polymer Science*, *132*, 42480–42490.

Nofar, M., Heuzey, M-C., Carreau, P. J., & Kamal, M. R. (2016). Effects of nanoclay and its localization on the morphology stabilization of PLA/PBAT blends under shear flow. *Polymer*, *98*, 353–364.

Oussalah, M., Caillet, S., Saucier, L., & Lacroix, M. (2007). Inhibitory effects of selected plant essential oils on the growth of four pathogenic bacteria: *E. coli* O157: H7, *Salmonella* Typhimurium, *Staphylococcus aureus* and *Listeria monocytogenes*. *Food Control, 18*, 414–420.

Perdikaki, A., Galeou, A., Pilatos, G., Karatasios, I., Kanellopoulos, N. K., Prombona, A., & Karanikolos, G. N. (2016). Ag and Cu monometallic and Ag/Cu bimetallic nanoparticle–graphene composites with enhanced antibacterial performance. *ACS Applied Materials & Interfaces*, *8*, 27498–27510.

Pluta, M. (2004). Morphology and properties of polylactide modified by thermal treatment, filling with layered silicates and plasticization. *Polymer, 45*(24), 8239–8251.

Qin, Y., Liu, D., Wu, Y., Yuan, M., Li, L., & Yang, J. (2015). Effect of PLA/PCL/cinnamaldehyde antimicrobial packaging on physicochemical and microbial quality of button mushroom (*Agaricus bisporus*). *Postharvest Biology and Technology, 99*, 73–79.

Qin, Y., Li, W., Liu, D., Yuan, M., & Li, L. (2017). Development of active packaging film made from poly (lactic acid) incorporated essential oil. *Progress in Organic Coatings*, *103*, 76–82.

Qu, P., Gao, Y., Wu, G., & Zhang, L. (2010). Nanocomposites of poly (lactic acid) reinforced with cellulose nanofibrils. *BioResources*, *5*, 1811–1823.

Rana, D., Mandal, B. M., & Bhattacharyya, S. N. (1996). Analogue calorimetric studies of blends of poly (vinyl ester) s and polyacrylates. *Macromolecules*, *29*, 1579–1583.

Rana, D., Mandal, B. M., & Bhattacharyya, S. N. (1993). Miscibility and phase diagrams of poly (phenyl acrylate) and poly (styrene-co-acrylonitrile) blends. *Polymer, 34*, 1454–1459.

Rhim, J. W., Park, H. M., & Ha, C. S. (2013). Bio-nanocomposites for food packaging applications. *Progress in Polymer Science*, *38*(10), 1629–1652.

Rojas-Graü, M. A., Avena-Bustillos, R. J., Friedman, M., Henika, P. R., Martín-Belloso, O., & McHugh, T. H. (2006). Mechanical, barrier, and antimicrobial properties of apple puree edible films containing plant essential oils. *Journal of Agricultural and Food Chemistry*, *54*(24), 9262–9267.

Sanla-Ead, N., Jangchud, A., Chonhenchob, V., & Suppakul, P. (2012). Antimicrobial activity of cinnamaldehyde and eugenol and their activity after incorporation into cellulose-based packaging films. *Packaging Technology & Science*, *25*, 7–17.

Scandorieiro, S., de Camargo, L. C., Lancheros, C. A., Yamada-Ogatta, S. F., Nakamura, C. V., & de Oliveira, A. G. (2016). Synergistic and additive effect of oregano essential oil and biological silver nanoparticles against multidrug-resistant bacterial strains. *Frontiers in Microbiology*, *23*(7), 760. https://doi.org/10.3389/fmicb.2016.00760.

Sothornvit, R., Hong, S. I., An, D. J., & Rhim, J. W. (2010). Effect of clay content on the physical and antimicrobial properties of whey protein isolate/organo-clay composite films. *LWT - Food Science and Technology*, *43*, 279–284.

Sung, S. H., Chang, Y., & Han, J. (2017). Development of polylactic acid nanocomposite films reinforced with cellulose nanocrystals derived from coffee silverskin. *Carbohydrate Polymers*, *169*, 495–503.

Tan, K. S., & Cheong, K. Y. (2013). Advances of Ag, Cu, and Ag-Cu alloy nanoparticles synthesized via chemical reduction route. *Journal of Nanoparticle Research*, *15*, 4.

Taner, M., Sayar, N., Yulug, I. G., & Suzer, S. (2011). Synthesis, characterization and antibacterial investigation of silver-copper nanoalloys. *Journal of Materials Chemistry*, *21*, 13150–13154.

Tawakkal, I. S., Cran, M. J., Miltz, J., & Bigger, S. W. (2014). A review of poly (lactic acid)-based materials for antimicrobial packaging. *Journal of Food Science*, *79*, R1477–90.

Varshney, R., Bhadauria, S., & Gaur, M. S. (2010). Characterization of copper nanoparticles synthesized by a novel microbiological method. *Journal of The Minerals, Metals & Materials Society*, *62*, 102–104.

Yahyaoui, M., Gordobil, O., Díaz, R. H., Abderrabba, M., & Labidi, J. (2016). Development of novel antimicrobial films based on poly (lactic acid) and essential oils. *Reactive and Functional Polymers*, *109*, 1–8.

Zain, N. M., Stapley, A. G. F., & Shama, G. (2014). Green synthesis of silver and copper nanoparticles using ascorbic acid and Chitosan for antimicrobial applications. *Carbohydrate Polymers*, *112*, 195–202.

Zhu, J. Y., Tang, C. H., Yin, S. W., & Yang, X. Q. (2018). Development and characterization of novel antimicrobial bilayer films based on polylactic acid (PLA)/pickering emulsions. *Carbohydrate Polymers*, *181*, 727–735.

Zhuang, W., Liu, J., Zhang, J. H., Hu, B. X., & Shen, J. (2009). Preparation, characterization, and properties of TiO_2/PLA nanocomposites by in situ polymerization. *Polymer Composites*, *30*, 1074–1080.